https://doi.org/10.5194/egusphere-2026-1883
Preprint. Discussion started: 10 April 2026

First Observations of the Solar-Heating Imprint on Seasonal Variations in Diurnal Tidal Structure in the MLT Region

Wen Yi[1,2,3], Jianyuan Wang[4], Xianghui Xue[1,2,3,5], Chengyun Yang[1,3], Iain M. Reid[6,7], Robert A. Vincent[6,7], Andrew MacKinnon[7], Damian J. Murphy[8], Njål Gulbrandsen[9], Masaki Tsutsumi[10], Baiqi Ning[11], Guozhu Li[11], Nicholas J. Mitchell[12,13], Tracy Moffat-Griffin[13], Toshitaka Tsuda[14], Alan Z. Liu[15], Zishun Qiao[16], Haiying Li[17], Paulo P. Batista[18], Jianfei Wu[1,3], Tingdi Chen[1,3] , Xiankang Dou[1,5]

[1]CAS Key Laboratory of Geospace Environment, School of Earth and Space Sciences, University of Science and Technology of China, Hefei, China,
[2]State Key Laboratory of Environment Characteristics and Effects for Near-space, Beijing, China,
[3]CAS Center for Excellence in Comparative Planetology, Anhui Mengcheng Geophysics National Observation and Research Station, University of Science and Technology of China, Hefei, China
[4]School of Microelectronics, Tianjin University, Tianjin, China,
[5]Hefei National Laboratory, University of Science and Technology of China, Hefei, China
[6]ATRAD Pty Ltd., Underdale, South Australia, Australia,
[7]School of Physical Sciences, University of Adelaide, Adelaide, South Australia, Australia
[8]Australian Antarctic Division, Kingston, Tasmania, Australia
[9]Tromsø Geophysical Observatory, UiT – The Arctic University of Norway, Tromsø, Norway
[10]National Institute of Polar Research, Tachikawa, Japan
[11]Key Laboratory of Earth and Planetary Physics, Institute of Geology and Geophysics, Chinese Academy of Sciences, Beijing, China
[12]British Antarctic Survey, Cambridge, UK
[13]Department of Electronic & Electrical Engineering, The University of Bath, UK
[14]Research Institute for Sustainable Humanosphere (RISH), Kyoto University, Uji, Japan
[15]Center for Space and Atmospheric Research, Department of Physical Sciences, Embry-Riddle Aeronautical University, Daytona Beach, Florida, USA
[16]High Altitude Observatory, NSF National Center for Atmospheric Research, Boulder, Colorado, USA
[17]National Key Laboratory of Electromagnetic Wave Propagation, China Research Institute of Radiowave Propagation, Qingdao, China
[18]Heliophysics, Planetary Science and Aeronomy Division, National Institute for Space Research-INPE, São José dos Campos, SP, Brazil

Keywords: Diurnal Tides, Mesosphere and Low Thermosphere, Meteor Radar, Solar Zenith Angle

Corresponding author: Xianghui Xue (xuexh@ustc.edu.cn)

https://doi.org/10.5194/egusphere-2026-1883
Preprint. Discussion started: 10 April 2026

Abstract: A global climatology of diurnal tides in the mesosphere and lower thermosphere (MLT) is constructed using multiyear observations from fifteen meteor radars distributed worldwide. The results show that diurnal tidal amplitudes are strongest at low and mid-latitudes (10°–50° N/S), with peak values of about 60 m s^{-1} near 20°–30° N/S, and are comparatively weak near the Equator and at polar latitudes. The seasonal variations of the diurnal tide are characterized by maxima around the equinoxes and minima during the solstices. In addition to these global climatological features, we identify a clear modulation of the vertical structure of diurnal tidal amplitude and phase by seasonal variations in solar forcing, represented here by the solar zenith angle (SZA). This modulation is particularly evident at northern low and mid-latitudes, but is much weaker in the Southern Hemisphere. The hemispheric asymmetry suggests that the tidal response to solar forcing is not globally uniform. To further explore the possible cause of this asymmetry, we examine the meridional fluxes of zonal tidal momentum. The results suggest that background zonal winds can influence tidal propagation through filtering effects and momentum drag, thereby contributing to the observed hemispheric differences in tidal structure. These results provide new observational evidence for the coupling between solar forcing and diurnal tides in the MLT region and offer useful constraints for the evaluation of general circulation models. They also improve our understanding of tidal propagation and variability in the middle and upper atmosphere.

Introduction

The global wind field, temperature, density, and atmospheric composition of the mesosphere and lower thermosphere (MLT) region are strongly influenced by the vertical upward propagation of atmospheric (solar) tides that transport energy and momentum from the lower atmosphere to the middle and upper atmosphere (see, e.g., Forbes and Garret, 1979; Forbes, 1995; Hagan and Forbes, 2002; Manson et al., 2004; Pancheva et al., 2014). Atmospheric tides in the MLT region are important components of the general circulation (Hagan and Forbes, 2002, Smith, 2012; Becker, 2017).

Ground-based and satellite techniques are widely used to observe atmospheric tides in

https://doi.org/10.5194/egusphere-2026-1883
Preprint. Discussion started: 10 April 2026

the MLT region. Both of these techniques have their own advantages and limitations. As tides are global-scale oscillations with periods that are harmonics of a solar day, satellite observations can capture both migrating and nonmigrating components (Hagan and Forbes, 2002; Manson et al., 2004; Oberheide et al., 2006; Wu et al., 2008a, 2008b; Mukhtarov et al., 2009; Xu et al., 2009; Pancheva et al., 2009, 2010; and the references therein). However, the limitations of satellite techniques are that their inclination precessing orbits basically take dozens of days to cover the whole day in local time. For example, the thermosphere, ionosphere, mesosphere energetics, and dynamics (TIMED) satellite needs 60 days to cover 24-hour measurements, so observations based on satellite techniques can usually provide the climatology of the slowly varying global-scale migrating and nonmigrating tides (Xu et al., 2009; Pancheva et al., 2009), but they are not well suited for investigating short-term variability in regional tides.

In addition to space-based observations, an advantage of ground-based techniques, such as meteor radar (MR) and medium frequency (MF) radar, is high temporal resolution of MLT tides, which in the last few decades have been successfully used for investigating the short-term variability and seasonal, intraseasonal and interannual variations in tides, as well as their long-term trend changes at various geographic locations (e.g., Manson et al., 1999, 2002, 2004; Jacobi et al., 1999; Riggin et al., 1999; Vincent et al., 1998; Mitchell et al., 2002; Pancheva et al., 2020; Yi et al., 2019, 2023; Stober et al., 2021a; Hindley et al., 2022; Wang et al., 2022; Zhou et al., 2022). The obvious limitation of a single station is its inability to resolve the global-scale oscillation of tides and extract migrating and nonmigrating tides.

To achieve the decomposition of tidal components, a few studies have used the longitudinal distribution of MRs and MFs at particular latitudes to resolve migrating and nonmigrating tidal components (e.g., Murphy, 2003; Murphy et al., 2006; He et al., 2018; He and Chau, 2019; Liu et al., 2020; Wang et al., 2022). However, in the last few decades, numerous studies have investigated mesospheric tides, which were often limited to a single station or particular latitudes (e.g., Manson et al., 2002; Davis et al., 2013; Stober et al., 2021a; 2021b; and the references therein). Therefore, the global

https://doi.org/10.5194/egusphere-2026-1883
Preprint. Discussion started: 10 April 2026

picture of mesospheric tides observed by ground-based radars is still sparse.

Diurnal tides exhibit variability across a wide range of timescales, from days to years, primarily driven by two mechanisms: (1) variability in tropospheric and stratospheric tidal forcing (Zhang et al., 2010; Lieberman et al., 2007), and (2) amplitude modulation through interactions with the mean flow, planetary waves, and gravity waves (McLandress, 2002a, 2002b; Becker, 2017). Long-term variations in diurnal tides are further influenced by seasonal cycles, interannual phenomena such as the El Niño–Southern Oscillation (ENSO), the quasi-biennial oscillation (QBO), and the 11-year solar cycle. These factors affect both the generation and vertical propagation of tides by modulating tropospheric heating and background wind structures (Vincent et al., 1998; Lieberman et al., 2007; Hindley et al., 2022; Ramesh et al., 2024; Sheng et al., 2025).

The current global distribution of meteor radars, spanning from the northern to southern polar regions, provides favorable spatial and temporal coverage for investigating the climatology of mesospheric tides. In this study, we present a global view of diurnal tidal amplitudes and phases based on observations from fifteen meteor radars. Our results demonstrate that solar heating strongly influences the seasonal evolution of the vertical structure of diurnal tidal amplitudes and phases. In addition, using horizontal wind measurements, we examine the coupling between tides and the mean flow, which modulates the amplitude, phase, and vertical wavelength of diurnal tides. These findings provide compelling evidence that solar forcing plays a significant role in shaping the behavior of diurnal tides in the MLT region.

2. Data and Method

In this study, hourly horizontal wind data from fifteen meteor radars (MR) are used. The locations of the stations and their abbreviations are shown in Figure 1. Further information summarizing geographic locations, operational frequencies, peak powers, and observational periods is available in Table 1. All meteor radars used in this study are manufactured either by ATRAD Ltd. (Holdsworth et al., 2004) or by Genesis Ltd. (Hocking et al., 2001), which have very similar designs and operation principles. The

https://doi.org/10.5194/egusphere-2026-1883
Preprint. Discussion started: 10 April 2026

DVMR, BPMR, DWMR, FKMR, KMMR, WHMR, BJMR, MCMR, MHMR, TRMR, and SVMR manufactured by ATRAD Ltd. provide temporal and altitudinal resolutions of 1 hr and 2 km. The KTMR, ASSMR, ALOMR, and KEPMR manufactured by Genesis Ltd. provide temporal and altitudinal resolutions of 1 hr and 3 km. To better use these data for fitting tidal components, the vertical resolution of horizontal wind data was calculated every 2 km within the altitude range from 80 to 100 km. Reid et al. (2018) and Zeng et al. (2022) carried out joint measurement campaigns involving two meteor radars located at Davis Station in Antarctica and Kunming Station at low latitudes, respectively, summarized the performance of wind measurements observed by meteor radar and provided a precise estimation of wind uncertainties.

Table 1. Main operation parameters, geographic coordinates and observational time periods for the meteor radars used in this study.

	Meteor radars	Geographic coordinates	Frequency	Peak Power	Included date range	Approx. Years
Southern Hemisphere (SH)	Davis (DVMR)	68.6°S, 77.9°E	33.2 MHz	7.5 kW	2005-2024	20
	King Edward Point (KEPMR)	54.3° S, 36.5°W	35.2 MHz	7.5 kW	2016-2020	5
	Buckland Park (BPMR)	34.6°S, 138.5°E	55 MHz	40 kW	2016-2021	5
	Andes Lidar Observatory (ALOMR)	30.3°S, 70.7°W	35.2 MHz	7.5 kW	2009-2013	5
	Darwin (DWMR)	12.3°S, 130.8°E	33.2 MHz	7.5 kW	2006-2014	8
	Ascension Island (ASSMR)	7.9°S, 14.4° W	43.5 MHz	12 kW	2002-2011	10
	Kototabang (KTMR)	0.2°S, 100.3°E	37.7 MHz	12 kW	2003-2017	14
Northern Hemisphere (NH)	Fuke (FKMR)	19.5°N, 109.1°E	38.9 MHz	20 kW	2015-2020	6
	Kunming (KMMR)	25.6°N 103.8°E	37.5 MHz	20 kW	2011-2016	5
	Wuhan (WHMR)	30.5°N, 114.4°E	38.9 MHz	20 kW	2012-2024	13

https://doi.org/10.5194/egusphere-2026-1883
Preprint. Discussion started: 10 April 2026

	Mengcheng (MCMR)	33.4°N, 116.1°E	38.9 MHz	20 kW	2014-2024	11
	Beijing (BJMR)	40.3°N, 116.2°E	38.9 MHz	7.5 kW	2012-2023	12
	Mohe (MHMR)	53.5°N, 122.3°E	38.9 MHz	20 kW	2012-2024	13
	Tromsø (TRMR)	69.6°N, 19.2°E	30.3 MHz	7.5 kW	2004-2023	20
	Svalbard (SVMR)	78.2°N, 16.0°E	31 MHz	7.5 kW	2004-2023	20

To extract the tidal components observed by the meteor radars, we calculate the amplitude and phase of tidal components. The tidal analysis involves harmonics fitted to the hourly mean zonal and meridional winds. The fitting function is given by

$$y(t) = \bar{y}(t) + \sum_{i=1}^{3} A_i \sin\left(\frac{2\pi i}{24} t + \emptyset_i\right), \quad (1)$$

where $y(t)$ is the wind measurement, $\bar{y}(t)$ is the prevailing component, and A_i and $\emptyset_i$ represent the amplitude and phase, respectively. The tidal components with periods of 24 h, 12 h and 8 h represent the diurnal, semidiurnal and terdiurnal tides, respectively. As shown in Figure A1 in Supporting Information, we tested multiple fitting window lengths (5-day, 7-day, and 11-day) and found that the resulting diurnal amplitudes and phases were largely consistent across these window sizes. The choice of window length had minimal effect on the analysis of seasonal tidal variations. Based on this assessment, we adopted a 7-day window with a 1-day step to extract the 24 h, 12 h, and 8 h tidal components from the wind data using a least-squares fitting method over the 80–100 km altitude range.

https://doi.org/10.5194/egusphere-2026-1883
Preprint. Discussion started: 10 April 2026

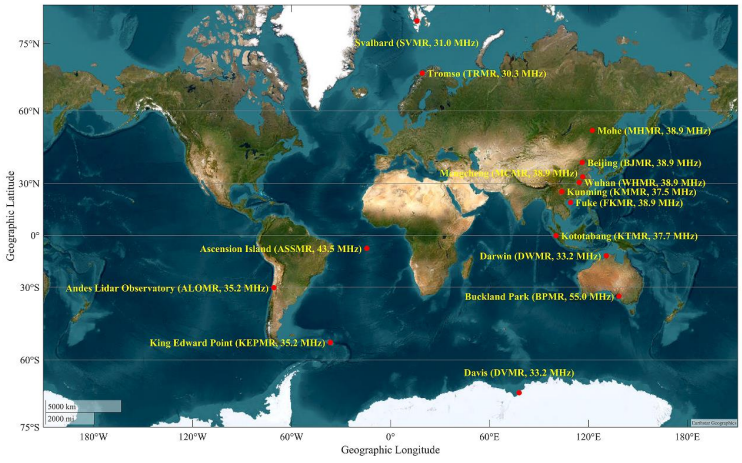

Figure 1. The locations of the Davis Station (DVMR, 68.6°S, 77.9°E), King Edward Point Station (KEPMR, 54° S, 36° W), Buckland Park (BPMR, 34.6°S, 138.5°E), Andes Lidar Observatory (ALOMR, 30.3° S, 70.7° W), Darwin (DWMR, 12.3° S, 130.5° E), Ascension Island (ASSMR, 7.9° S, 14.4° W), Kototabang (KTMR, 0.2°S, 100.3°E), Fuke (FKMR, 19.5°N, 109.1°E), Kunming (KMMR, 25.6°N 103.8°E), Wuhan (WHMR, 30.6° N, 114.4° E), Mengcheng (MCMR, 33.4° N, 116.5° E), Beijing (BJMR, 40.3° N, 116.2° E), Mohe (MHMR, 53.5° N, 122.3° E), Tromsø (TRMR, 69.6° N, 19.2° E), and Svalbard (SVMR, 78.2°N, 16°E).

The DT results are based on radar measurements with varying lengths of observational records. Some radars, such as ALOMR, KMMR, and KEPMR, have only 5 years of data, while others, like DVMR and TRMR, have up to 20 years. These differences in record length may influence the calculated mean DT amplitudes or the estimated tidal magnitudes. In Figures A2 and A3, we compare DT amplitudes and phases derived from 20 years and 5 years of data at the Davis meteor radar (DVMR). The comparison clearly shows that the differences between the two datasets are small, suggesting that data length does not significantly affect the climatological features of the diurnal tides presented in this study.

3. Results

3.1 Seasonal Variation of Global Diurnal Tides

Figure 2 presents the seasonal–altitude structures of monthly mean diurnal tidal (DT) amplitudes and phases in zonal and meridional winds from the southern to northern

https://doi.org/10.5194/egusphere-2026-1883
Preprint. Discussion started: 10 April 2026

polar regions. At polar latitudes, DT amplitudes from SVMR, TRMR, and DVMR show annual variation, peaking in summer and weakening in winter, with similar zonal and meridional patterns. In general, the DT amplitude during summer in both polar regions shows a relatively weak enhancement at lower altitudes below 84 km, reaching values up to 10 m/s, and a strong enhancement at higher altitudes above 96 km, reaching values up to 20 m/s. Stober et al. (2021b) reported that the DT amplitudes observed by the McMurdo meteor radar (77.8°S) at higher polar latitudes in the SH show stronger enhancements during summer in zonal components and have semiannual enhancements during March-May (autumn) and September-November (spring) in meridional components, which presents a different seasonal pattern of diurnal tides to the DVMR observations.

At higher northern midlatitudes, the zonal and meridional DT amplitudes observed by the MHMR show similar seasonal patterns with high latitude TRMR observations, reaching their maximum during summer with values up to 10 m/s. At southern higher midlatitudes, the KEPMR zonal DT amplitudes are very weak and show two weak enhancements in March (autumn) and September (spring), reaching values up to 10 m/s. The KEPMR meridional DT amplitudes are much stronger than those of the zonal component, which shows enhancements above 96 km with a maximum near the spring equinox, reaching values up to 20 m/s (e.g., Hindley et al., 2022). Although at the geographically conjugate higher mid-latitudes, the diurnal tide observed by the MHMR and KEPMR shows a clear seasonal asymmetry.

The DT amplitudes observed by the BJMR, MCMR, and WHMR from 40°N to 30°N at northern midlatitudes generally exhibit a similar seasonal pattern. They show a first enhancement near the spring equinox and a second enhancement around the autumn equinox. The DT amplitudes of the zonal components observed by the BJMR and MCMR, reaching values up to 30 m/s and 45 m/s, respectively, are stronger than the values of the meridional component, reaching up to 25 m/s and 35 m/s, respectively. At lower midlatitudes near 30° N, the WHMR zonal and meridional DT amplitudes are generally equal, reaching values up to 50 m/s.

https://doi.org/10.5194/egusphere-2026-1883
Preprint. Discussion started: 10 April 2026

At southern midlatitudes near 30°S, the DT amplitude observed by ALOMR exhibits two significant enhancements that appear near the spring and autumn equinoxes. At higher latitudes, the BPMR DT amplitude exhibits a strong enhancement near the autumn equinox and a second enhancement in the later autumn equinox. However, the seasonal morphology of diurnal tides two conjugate 30° latitudes shows a clear seasonal asymmetry, both peak in February–March, but ALOMR near autumn and MCMR near spring equinox. Furthermore, the ALOMR meridional DT amplitude is stronger than that of zonal components.

At northern low latitudes, the zonal and meridional DT amplitudes observed by the KMMR and FKMR exhibit two significant enhancements that appear in February-March and September-November. Different from the midlatitudes, the meridional DT amplitudes at low latitudes are stronger than those of the zonal component. Deepa et al. (2008) reported that the zonal and meridional DT amplitudes observed in the Trivandrum (8.5°N) meteor radar are maximum during autumn (August–November) and spring (March), and meridional amplitudes are stronger than zonal amplitudes, which are generally similar to the FKMR (19.5°N) observations.

https://doi.org/10.5194/egusphere-2026-1883
Preprint. Discussion started: 10 April 2026

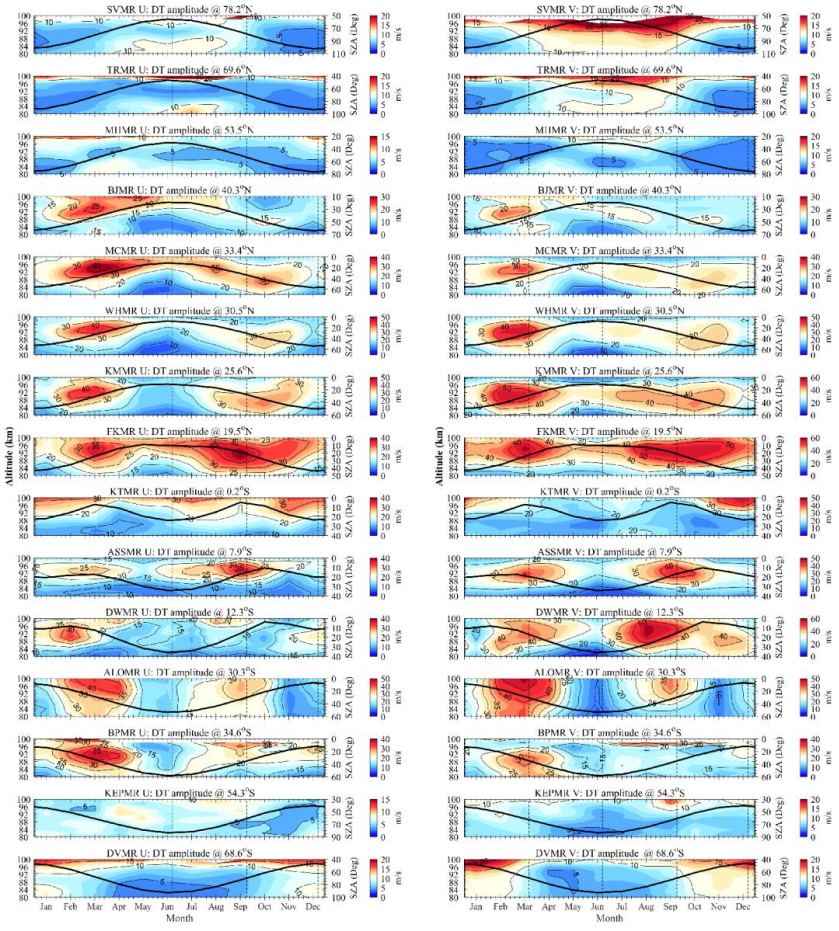

Figure 2. Monthly mean amplitudes of composite zonal (left column) and meridional (right column) diurnal tidal (DT) components derived from fifteen meteor radars. Note that the colorbar scales differ between panels. The black lines represent the solar zenith angle at local noon (1200 LT), corresponding to the right axes. Vertical black dashed lines indicate the spring and autumn equinoxes, as well as the summer and winter solstices.

At southern low latitudes, zonal DT amplitudes observed by the DWMR exhibit strong enhancement in summer (February) and weaker enhancement in spring (September). The Meridional DT amplitudes show two peaks—one in spring (September) and another during March–April. Zonal amplitudes from the ASSMR display semiannual variations, peaking near the equinoxes (September and March) (e.g., Davis et al., 2013). Meridional DT amplitudes from both DWMR and ASSMR show similar semiannual

https://doi.org/10.5194/egusphere-2026-1883
Preprint. Discussion started: 10 April 2026

patterns, with peak values reaching ~60 m/s in DWMR data. Kishore Kumar et al. (2014) also reported semiannual variations over Cachoeira Paulista (22°S), with meridional and zonal amplitude peaks of 55 m/s and 45 m/s, respectively—similar to ALOMR observations at 30°S. At the equator, KTMR data show three peaks: January–February, June–July, and November–December. These amplitudes increase with altitude, reaching ~40 m/s near 100 km.

Figure 3 presents the monthly mean phases of the zonal and meridional diurnal tides (DTs), defined as the time of the first positive maximum in the hourly wind measurements. Since the phases are calculated in local time, longitudinal differences among radars are eliminated. At high latitudes, SVMR and TRMR exhibit semiannual variations in both components, while DVMR displays annual variations, characterized by more stable phases and longer vertical wavelengths compared to SVMR and TRMR. At higher northern midlatitudes, the DT phases at MHMR resemble those at TRMR, with semiannual variation in the zonal component and annual variation in the meridional component. In contrast, KEPMR at southern midlatitudes shows semiannual variations in both components—differing from DVMR but similar to ALOMR and BPMR. The zonal DT phases at ALOMR exhibit weak annual variation, whereas the meridional phases are semiannual and more variable. For both BPMR and ALOMR, meridional vertical wavelengths are shorter in summer and longer in winter.

https://doi.org/10.5194/egusphere-2026-1883
Preprint. Discussion started: 10 April 2026

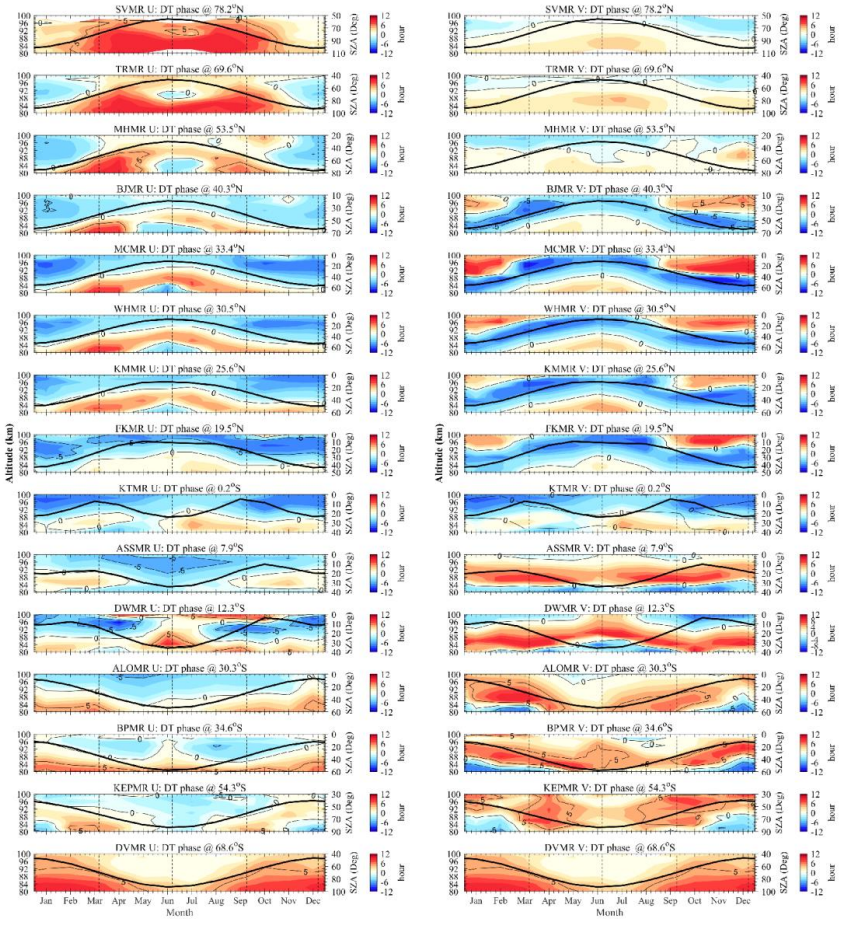

Figure 3. Same as Figure 2, but for the monthly mean phases of composite zonal (left column) and meridional (right column) diurnal tidal (DT) components

The zonal and meridional DT phases observed by the BJMR, MCMR, WHMR, KMMR, and FKMR from middle to lower latitudes in the NH generally exhibit similar seasonal characteristics. Both zonal and meridional DT phases remain stable throughout the year and are indicative of upward propagating tides. Their diurnal tidal vertical wavelengths during summer and winter are generally longer than those during spring and autumn. Note that this behavior is consistent with the Hough-mode decomposition shown in Lieberman et al. (2003, their Fig. 9) for the migrating diurnal tide: the (1, 2) mode maximizes near the equinoxes and has a vertical wavelength of ~15 km, whereas the (1,

https://doi.org/10.5194/egusphere-2026-1883
Preprint. Discussion started: 10 April 2026

1) mode exhibits a weak annual cycle and a longer vertical wavelength. There are approximately 3-6/6-12 hour phase lags between the zonal and meridional components during summer/winter. In the SH low latitudes (KTMR, ASSMR, DWMR), DT phases are also stable with small seasonal changes but show clear zonal–meridional differences. At the equator, KTMR zonal wavelengths shorten near equinox and lengthen in winter and spring. The ASSMR zonal DT phases at SH lower latitudes show similar seasonal variations with KTMR.

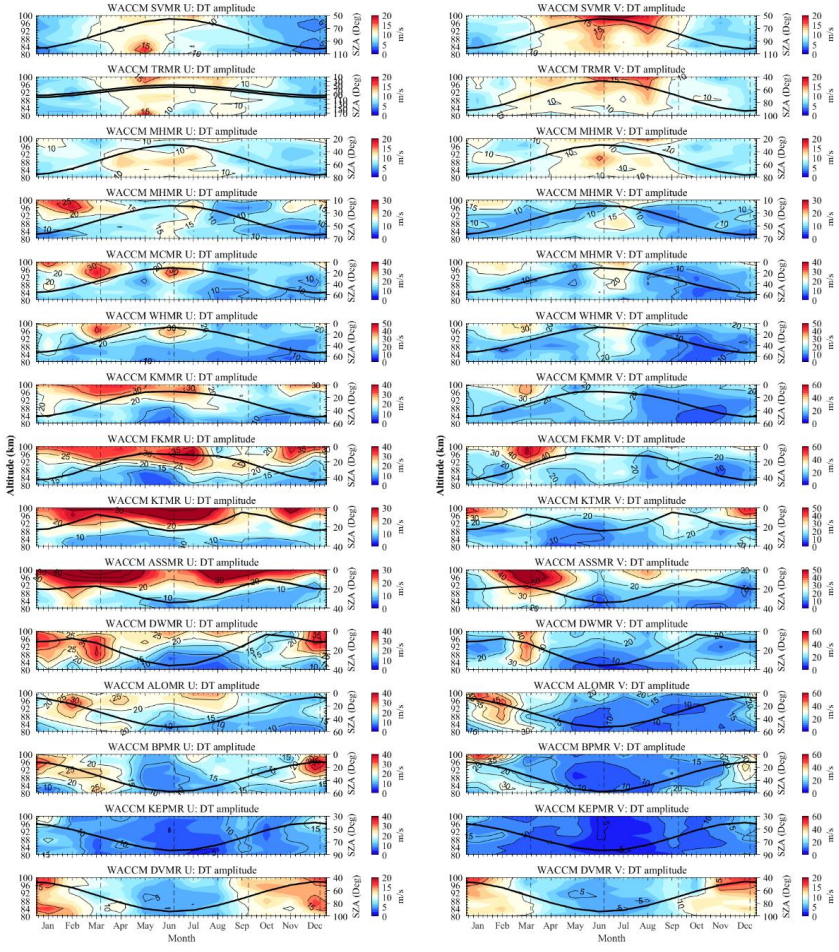

Figure 4 Same as Figure 2, but for the monthly mean amplitudes of composite zonal (left column) and meridional (right column) diurnal tidal (DT) components obtained from the SD-WACCM.

https://doi.org/10.5194/egusphere-2026-1883
Preprint. Discussion started: 10 April 2026

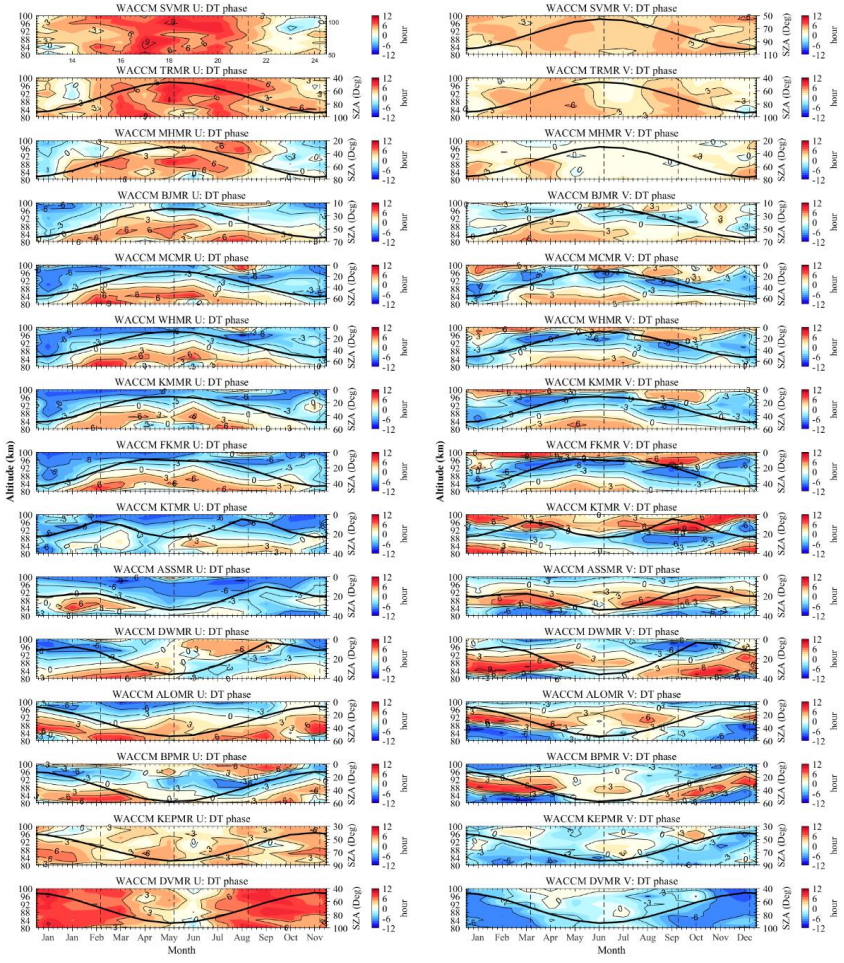

Figure 5. Same as Figure 3, but for the monthly mean phases of composite zonal (left column) and meridional (right column) diurnal tidal (DT) components obtained from the SD-WACCM.

3.2 **Influence of Solar Zenith Angle on Seasonal Diurnal Tides**

Figure 2 also shows seasonal variations of solar zenith angle (SZA) at 12 LT over fifteen meteor radars. In this study, we adopt the SZA at local noon (12:00 LT) as a representative value (e.g., Liu et al., 2019), since it closely reflects the maximum daily solar heating and captures the dominant seasonal trend relevant for atmospheric tidal excitation.

https://doi.org/10.5194/egusphere-2026-1883
Preprint. Discussion started: 10 April 2026

A clear correlation is observed between the SZA and the vertical height of diurnal tidal (DT) amplitude maxima, especially at northern midlatitudes (BJMR, MCMR, WHMR), and to a lesser extent at northern low latitudes (KMMR, FKMR). Near the equator, DT amplitudes at KTMR exhibit a semiannual variation that also appears to be linked to SZA. In the southern midlatitudes, the vertical variation of DT amplitudes at BPMR is also correlated with SZA, although the relationship is weaker compared to that in the Northern Hemisphere. Overall, global observations suggest that solar heating modulates the altitude of DT amplitude maxima at low and midlatitudes, but this effect exhibits a clear hemispheric asymmetry. As shown in Figure A4, the global semidiurnal tidal (SDT) amplitudes observed by the fifteen meteor radars do not show such SZA dependence.

Compared to the DT amplitudes, the seasonal variations of the DT phase shown in Figure 3 exhibit a stronger correspondence with seasonal changes in solar forcing, as represented by the noon SZA. This effect is most evident across lower and midlatitudes in the NH, particularly at MHMR, BJMR, MCMR, and WHMR. Similar but weaker signals are observed at KTMR near the equator, as well as at ALOMR and BPMR in the SH midlatitudes, indicating a hemispheric asymmetry in the influence of SZA on DT phase. As shown in Figure A5, and consistent with expectations, the phases of the semidiurnal tide (SDT) exhibit no clear relationship with SZA.

As shown in Figures A4 and A5, we also computed the diurnal tidal (DT) amplitude and phase from hourly winds simulated by the specified-dynamics version of the Whole Atmosphere Community Climate Model (SD-WACCM), sampled at the meteor-radar locations. The simulation is nudged toward the Goddard Earth Observing System Model, Version 5 (GEOS-5) reanalysis product (Rienecker et al., 2008). SD-WACCM reproduces the seasonal variation of DT amplitudes at high latitudes, with maxima in summer and minima in winter (Stober et al., 2021a). However, at low and midlatitudes it fails to capture the seasonal behavior of the diurnal tides observed by the meteor radars used in this study, consistent with the findings of Zhou et al. (2022).

We further examine whether SD-WACCM can reproduce the seasonal trend in the

https://doi.org/10.5194/egusphere-2026-1883
Preprint. Discussion started: 10 April 2026

vertical structure of DT amplitude and phase that is directly modulated by the solar zenith angle (SZA). As expected, SD-WACCM generally does not reproduce this SZA-related feature in DT amplitudes. In contrast, it largely captures the SZA modulation of DT phase at Northern Hemisphere midlatitudes. The discrepancies between the observations and SD-WACCM suggest that the excitation mechanisms and evolution processes of diurnal tides in the mesosphere–lower thermosphere (MLT) region are still not fully understood.

3.3 Discussion on Hemispheric Differences in Diurnal Tide Modulation by Solar Zenith Angle

Figure 6 presents latitude–seasonal contour plots of the zonal and meridional diurnal tidal (DT) amplitudes at 86 and 92 km, derived from fifteen meteor radars. Across the mesopause region, both components generally maximize at ~20–30° N/S, consistent with direct global tidal wind measurements from TIMED/TIDI that show low-latitude DT wind maxima near ~20–30° and around ~90 km (e.g., Oberheide et al. (2006); Wu et al. (2008a, 2008b)) and with multi-instrument tidal wind/temperature inferences from Huang et al. (2006). Overall, the meridional DT amplitudes tend to be stronger than the zonal components. Seasonally, zonal diurnal tides typically peak around the equinoxes and reach minima near the solstices. The global structure indicates that DT amplitudes are largely characterized by semiannual variations, though annual and intraseasonal components are also present (e.g., Das et al., 2013; Yi et al., 2019; Guharay et al., 2021). It is important to note that the DTs observed by single-station meteor radars represent a combination of migrating and nonmigrating tides, which cannot be easily separated. In some cases, nonmigrating components may even dominate over the migrating ones (Forbes and Garrett, 1979). Migrating diurnal tides are primarily driven by solar infrared absorption by tropospheric water vapor and ultraviolet absorption by zonal-mean ozone in the stratosphere and lower mesosphere (Chapman and Lindzen, 1970; Forbes and Garrett, 1979; Lieberman et al., 2003). In contrast, nonmigrating tides arise from more complex mechanisms, including zonally asymmetric thermal forcing (e.g., surface topography, localized heating, longitudinal solar heating variations) and

https://doi.org/10.5194/egusphere-2026-1883
Preprint. Discussion started: 10 April 2026

nonlinear interactions with stationary planetary waves (Hagan and Forbes, 2002; 2003). Accurate modeling of these tides requires consideration of a broad range of atmospheric processes—including radiative, chemical, and dynamical effects—such as the global distribution of latent heat, ozone, and water vapor; background temperature and winds; molecular and eddy diffusivity; gravity wave drag; and Newtonian cooling (Manson et al., 2002).

In Figures 6e and 6f, we present the seasonal and global variations of surface net solar radiation and surface latent heat flux, based on data from the European Centre for Medium-Range Weather Forecasts (ECMWF). As shown in Figure 6e, solar radiation input is primarily governed by the SZA, with solar heating peaking at midlatitudes near 30° and exhibiting similar seasonal patterns across all sites. The seasonal variation in latent heat release, shown in Figure 6f, is largely latitude-dependent—strongest around 15°, weaker near the equator and midlatitudes, and weakest at high latitudes. Latent heat flux tends to be stronger in the winter hemisphere than in the summer (Kubota et al., 2003; Zhang et al., 2018). These results suggest that the solar heating sources of tides are generally symmetric between hemispheres. However, this symmetry does not explain why the observed SZA modulation of diurnal tides, implying that other factors such as background winds or dynamical interactions may be involved.

https://doi.org/10.5194/egusphere-2026-1883
Preprint. Discussion started: 10 April 2026

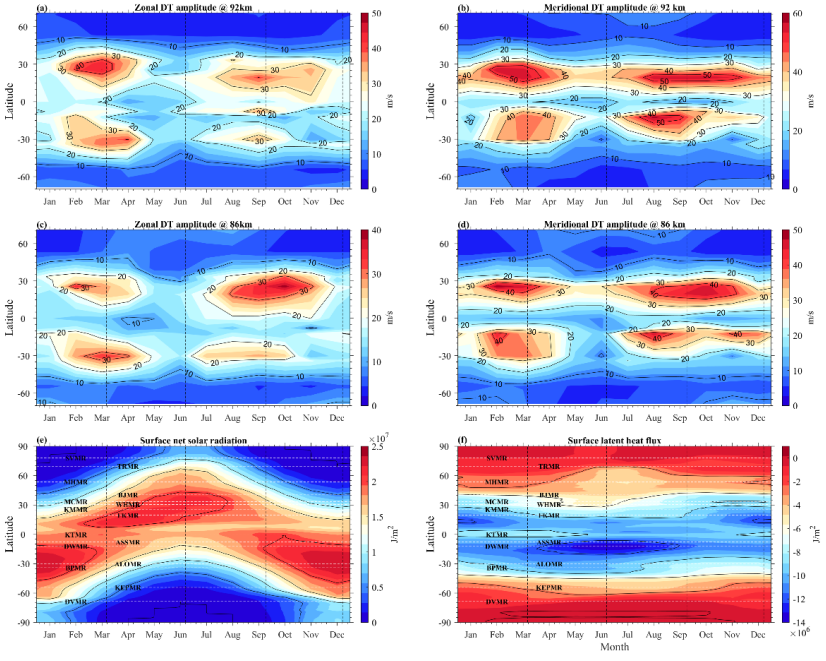

Figure 6 (a-d) Latitude-seasonal variations in the zonal and meridional diurnal tidal amplitudes at 92 and 86 km were obtained from the fifteen meteor radars. (e) and (f) Surface net solar radiation and Surface latent heat flux from ECMWF. Note that the values of colorbar are different.

https://doi.org/10.5194/egusphere-2026-1883
Preprint. Discussion started: 10 April 2026

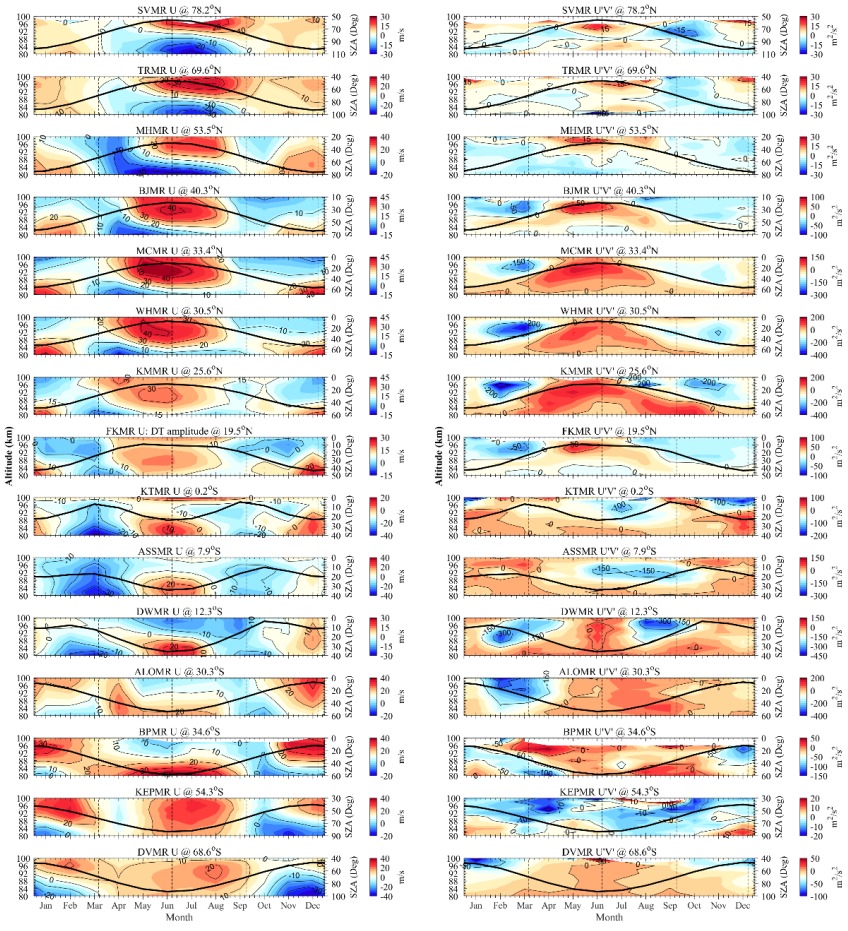

Figure 7. Comparison of background zonal wind (left column) and the meridional flux of tidal zonal momentum (right column) calculated by the fifteen meteor radars. Note that the colorbar values are different. The black lines depict the solar zenith angle at 12 LT noon, corresponding to the right axes. The vertical black dashed lines depict the spring and autumn equinoxes and summer and winter solstices.

In addition to the excitation sources, the influence of background circulation on tides should also be considered. The background zonal mean flow can affect the upward propagation process of tides through filtering effects, which can be interpreted as the background zonal mean flow exerting a drag on the zonal momentum of tides (e.g., McLandress, 2002b; Isoda et al., 2004; Liu et al., 2016). As previously noted, the WACCM simulation cannot fully resolve the seasonal variations of diurnal tides observed by meteor radars in this study, particularly at low- and mid-latitudes.

https://doi.org/10.5194/egusphere-2026-1883
Preprint. Discussion started: 10 April 2026

Therefore, it is necessary to identify a variable calculable from meteor radar observations to characterize variations in the zonal momentum of diurnal tides. The meridional flux of tidal zonal momentum can be derived using zonal and meridional wind tides, which is given as follows (Devara and Ahmed, 1986):

$$\overline{u'v'} = \frac{1}{2}\hat{u}\hat{v}cos(\phi_u - \phi_v) \quad (2)$$

Where $\overline{u'v'}$ denotes the meridional flux of tidal zonal momentum; $\hat{u}$ and $\hat{v}$ represent the amplitude of zonal wind tide and meridional tide, respectively; ϕ_u and ϕ_v denote the phase of zonal wind tide and meridional tide, respectively.

Figure 7 presents the comparison of background zonal wind and the meridional flux of tidal zonal momentum calculated by the fifteen meteor radars. It is noted that in observations from BJMR, MCMR, WHMR, KMMR, and FKMR located in mid-latitudes in the Northern Hemisphere, the SZA consistently aligns with the altitude and month where the background zonal wind reaches the maximum of the eastward direction and the diurnal tidal zonal momentum approaches zero. When the magnitude of the meridional flux of zonal momentum approaches zero, the vertical gradient of this meridional flux reaches its maximum. Since the (1,1) Hough mode of zonal wind diurnal tides peaks at approximately 25° of latitude, while the (1,1) Hough mode of meridional wind peaks around 20° of latitude, the diurnal tides in mid-latitude regions are primarily governed by the (1,1) mode of migrating tides with westward propagating zonal wavenumber 1. When the background eastward wind attains its maximum intensity, the filtering effect of the background mean flow allows substantial penetration of westward propagating tidal components, thereby maximizing the vertical gradient of momentum flux associated with these westward propagating tidal components. It should be noted that, at present, we have not yet separated the migrating and non-migrating tidal components from the single-station meteor radar wind observations. In future work, we plan to extract tidal components from the sounding of atmosphere using broadband emission radiometry (SABER) temperature data and further investigate the responses of different diurnal tidal components to solar forcing, particularly the SZA.

However, in the southern hemisphere, the consistency between the eastward maximum

https://doi.org/10.5194/egusphere-2026-1883
Preprint. Discussion started: 10 April 2026

of the background zonal wind and the zero-line of diurnal tidal zonal momentum is only observed in BPMR although ALOMR is also located at mid-latitude in the southern hemisphere. This suggests that the possible mechanism in BPMR may resemble that in northern hemisphere mid-latitudes, while ALOMR exhibits distinct behavior. Although ALOMR and BPMR share similar latitudes, BPMR is situated in Australia, whereas ALOMR is located near the Andes Mountains in South America. Beyond the filtering effects of the background mean flow on tides, gravity waves may also interact with tidal components (e.g., Liu and Hagan, 1998; Li et al., 2009; Stober et al., 2021b). The Andes Mountains near ALOMR generate strong topographic gravity waves with varying seasonal characteristics (e.g., Alexander and Teitelbaum, 2011; Cao et al., 2016; Randall et al., 2017; Llamedo et al., 2019), which could modify tidal amplitudes and phases, leading to deviations in the seasonal variations of tides from the SZA.

4. Conclusion

In Section 3, we show the climatology of global diurnal tides in the MLT region observed by fifteen meteor radars, especially the modulation of mesospheric tides by solar heating, which can be briefly summarized as follows:

1. In general, the diurnal tides are strong at lower and middle latitudes (10-50°N/S), reaching maxima near 20-30°N/S with values of approximately 60 m/s, and are weak at the equator and higher mid- and polar latitudes (higher than 50°N/S).

2. In terms of seasonal variation, the diurnal tides at lower and mid-latitudes generally reach the maximum near equinoxes and have smaller amplitudes during summer and winter solstices. In the equatorial region, the diurnal tides show enhancements during January-February, June-August, and October-November. In the polar region, the diurnal tides show enhancements during summer and are weak during winter.

3. The seasonal trend in the vertical altitude structure of the DT amplitude and phase is directly modulated by solar heating at northern lower and mid-latitudes, but in the Southern Hemisphere, the phenomenon is less pronounced. These differences reflect hemispheric asymmetry between the Northern and Southern Hemispheres.

4. Global distributions of meridional fluxes of zonal tidal momentum highlight the

https://doi.org/10.5194/egusphere-2026-1883
Preprint. Discussion started: 10 April 2026

critical role of background zonal winds in modulating tidal propagation. These winds can selectively filter tidal components and exert momentum forcing (or drag), thereby influencing both the amplitude and phase of the diurnal tide. This zonal wind–tide interaction is recognized as a primary mechanism contributing to the interhemispheric asymmetry observed in global tidal structures.

In conclusion, this study provides the first comprehensive global picture of diurnal tides observed by ground-based radars. Our results offer a new reference data set that can serve as a benchmark for future model development and evaluation of diurnal tides in the MLT region. The pronounced signatures of solar-heating-driven tides highlight persistent deficiencies in current models and underscore the need to better represent the underlying dynamical processes that link the lower atmosphere to the MLT region.

Appendix A: Comparison of Meteor Radar Tidal Estimations with Different Time Windows and Global Observations of the Semidiurnal Tide by Meteor Radars

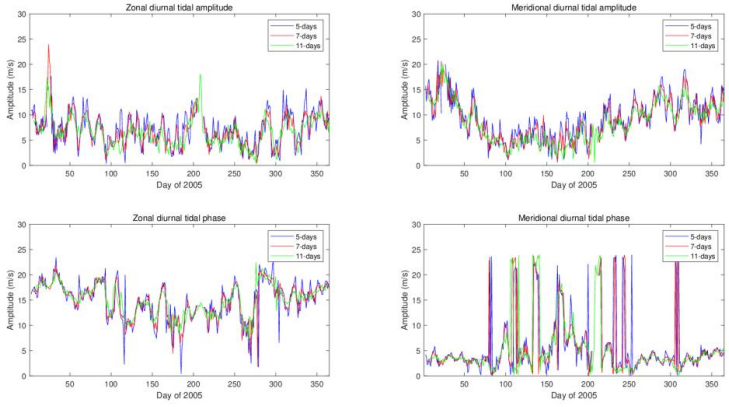

Figure A1. Zonal (left column) and meridional (right column) diurnal tide amplitudes (upper row) and phases (lower row) observed by the Svalbard Meteor Radar (SVMR) during 2005. The tidal amplitudes and phases are derived using sliding windows of 5 days (blue lines), 7 days (red lines), and 11 days (green lines).

https://doi.org/10.5194/egusphere-2026-1883
Preprint. Discussion started: 10 April 2026

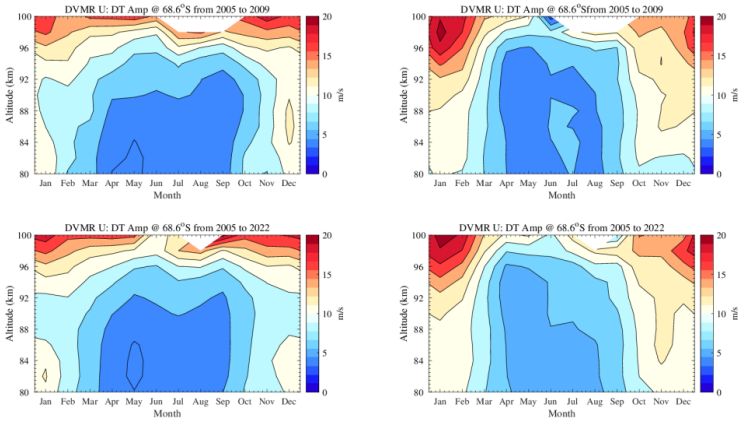

459

460 **Figure A2.** Zonal and meridional diurnal tide amplitude (left column) and phase (right
461 column) observed by the Davis Meteor Radar (DVMR). Results derived from 2005–
462 2022 are shown in the upper row, and those from 2005–2009 in the lower row.

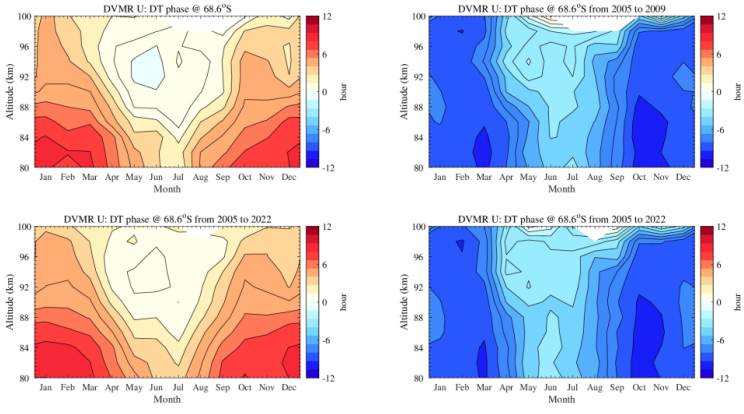

463

464 **Figure A3.** Same as A2, but for the meridional amplitude and phase.

https://doi.org/10.5194/egusphere-2026-1883
Preprint. Discussion started: 10 April 2026

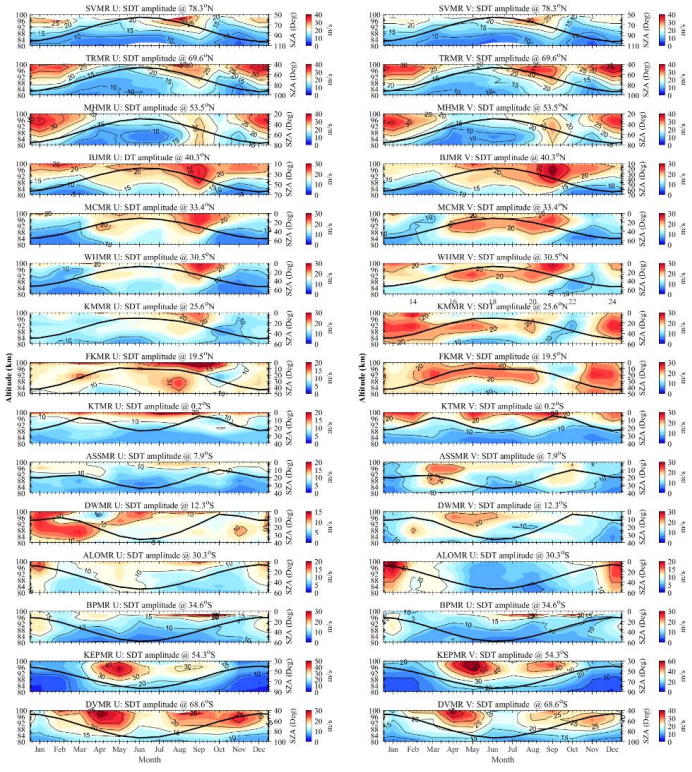

Figure A4. Monthly mean amplitudes of the composite zonal (U; left columns) and meridional (V; right columns) semidiurnal tidal (SDT) components derived from fifteen meteor radars. Note that the color-bar scales differ among panels. The black solid lines denote the solar zenith angle at local noon (1200 LT), shown on the right axes. The vertical black dashed lines indicate the spring and autumn equinoxes and the summer and winter solstices.

https://doi.org/10.5194/egusphere-2026-1883
Preprint. Discussion started: 10 April 2026

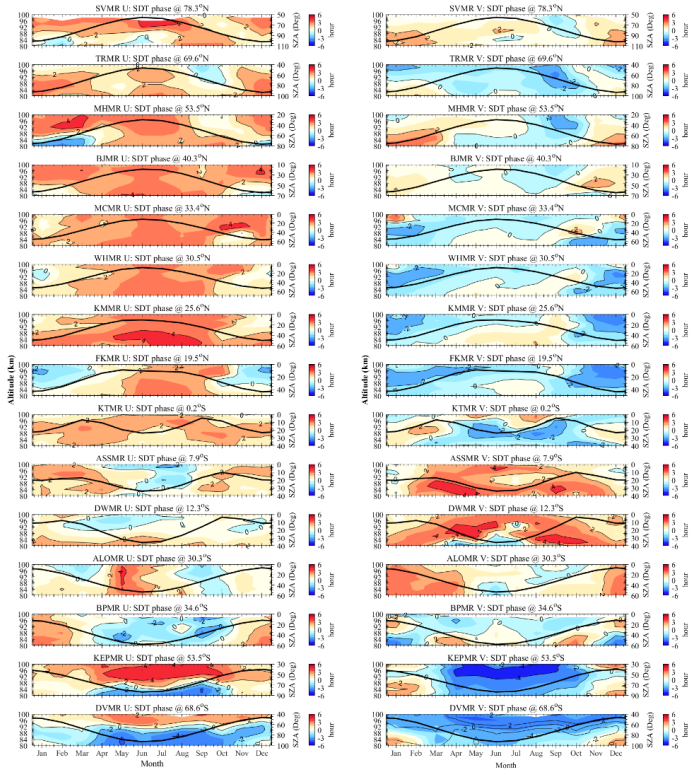

Figure A5. Same as Figure A4, but for the monthly mean phases of composite zonal (left column) and meridional (right column) semidiurnal tidal (SDT) components derived from fifteen meteor radars.

Data Availability Statement

The analyzed data presented in this manuscript are available at https://doi.org/10.6084/m9.figshare.29648918.v1 (Yi, 2025). The SD-WACCM dataset utilized in this study is available at https://doi.org/10.12176/01.60.00003-V01. The Surface net solar radiation and Surface latent heat flux dataset is available at https://www.ecmwf.int/en/forecasts/dataset/ecmwf-reanalysis-v5.

Author contributions

Conceptualization: WY, XX; data curation: XX, IMR, RAV, AM, DJM, NG, MT, BN, GL, NJM, TMG, TT, AL, ZQ, JC, PPB and JC; formal analysis: WY, JYW and CY; funding acquisition: WY, XX, and JW; investigation: WY; methodology: WY and JYW; project administration: XX and WY, resources: WY and XX; software: WY and JYW; supervision: XX and WY; validation: WY and XX; visualization: WY; writing – original draft preparation: WY; and writing – review and editing:WY, JYW and DJM. All authors have read and agreed to the published version of the paper.

https://doi.org/10.5194/egusphere-2026-1883
Preprint. Discussion started: 10 April 2026

Acknowledgements

This work has been supported by the B-type Strategic Priority Program of CAS (grant no. XDB0780000); the National Natural Science Foundation of China (Grant 42125402, 42574213 and 42304165); the National Key Technologies R&D Program of China (Grant 2022YFF0503703); the Chinese Meridian Project; the Fundamental Research Funds for the Central Universities; the State Key Laboratory of Environment Characteristics and Effects for Near-space (No.2025NS02); the Joint Open Fund of Mengcheng National Geophysical Observatory (MENGO-202406, MENGO- 202407). This research was supported by the International Space Science Institute (ISSI) in Bern, through ISSI International Team project #23–580 "Meteors and phenomena at the boundary between Earth's atmosphere and outer space". The operation of the Davis meteor radar was supported by Australian Antarctic Science Projects 2668, 4025, 4445, and 4637. The Svalbard meteor radar is supported by the Research Council of Norway under the project Svalbard Integrated Arctic Earth Observing System—Infrastructure development of the Norwegian node (SIOS-InfraNor, Project No. 269927).

References

Alexander, M. J., and H. Teitelbaum (2011) Three-dimensional properties of Andes mountain waves observed by satellite: A case study, J. Geophys. Res., 116, D23110, doi:10.1029/2011JD016151.

Becker, E., 2017: Mean-Flow Effects of Thermal Tides in the Mesosphere and Lower Thermosphere. J. Atmos. Sci., 74, 2043–2063, https://doi.org/10.1175/JAS-D-16-0194.1.

Cao, B., C. J. Heale, Y. Guo, A. Z. Liu, and J. B. Snively (2016), Observation and modeling of gravity wave propagation through reflection and critical layers above Andes Lidar Observatory at Cerro Pachón, Chile, J. Geophys. Res. Atmos., 121, 12,737–12,750, doi:10.1002/2016JD025173.

Cen, Y. (2022). 1979–2014 SDWACCM data [Dataset]. Figshare. https://doi.org/10.6084/m9.figshare.19777918

Chapman, S., Lindzen, R.S. (1970). Atmospheric tides: thermal and gravitational. Gordon and Breach, New York, NY, 200 pp.

Das S S, Kumar K K, Ramkumar G. (2013). First observations of quasi 120 day oscillation in mesospheric winds and temperature: Observations inferred from meteor radar. Radio Sci., 48: 310–315.

Devara, P. C. S., Ahmed, M. I. (1986). Momentum flux variations at lower thermospheric levels as seen from mid-latitude meteor wind observations. Meteorl. Atmos. Phys. 35, 236–241. https://doi.org/10.1007/BF01041816.

Davis, R. N., Du, J., Smith, A. K., Ward, W. E., and Mitchell, N. J. (2013). The diurnal and semidiurnal tides over Ascension Island (8 ° S, 14 ° W) and their interaction with the stratospheric quasi-biennial oscillation: studies with meteor radar, eCMAM and WACCM, Atmos. Chem. Phys., 13, 9543–9564, https://doi.org/10.5194/acp-13-9543-2013.

https://doi.org/10.5194/egusphere-2026-1883
Preprint. Discussion started: 10 April 2026

Deepa, V., Ramkumar, G., Antonita, M., Kumar, K. K. (2008). Meteor wind radar observations of tidal amplitudes over a low-latitude station Trivandrum (8.5 °N, 77 °E): Interannual variability and the effect of back ground wind on diurnal tidal amplitudes. J. Atmos. Sol.-Terr. Phys. 70: 2005-2013.

Forbes, J. M., and Garrett, H. B. (1979). Theoretical Studies of Atmospheric Tides. Rev. Geophys. Space Phys., 17, 1951-1981.

Forbes, J. M. Johnson, R. M. & Killeen, T. L. (Eds.) Tidal and Planetary Waves. The Upper Mesosphere and Lower Thermosphere: A Review of Experiment and Theory, American Geophysical Union, 1995, 67-87.

Guharay A, Batista P P, Buriti R A. (2021). Observations of a quasi-90-day oscillation in the MLT winds and tides over an equatorial station using meteor radar winds. Advances in Space Research, 67(10): 3125–3133.

Hagan, M. E., Burrage, M. D., Forbes, J. M., Hackney, J., Randel, W. J., Zhang, X. (1999). GSWM-98: Results for migrating solar tides. J Geophys Res., 104(A4), 6813–6827, doi:10.1029/1998JA900125.

Hagan, M. E., and Forbes, J. M. (2002). Migrating and nonmigrating diurnal tides in the middle and upper atmosphere excited by tropospheric latent heat release. J. Geophys. Res., 107(D24), ACL 6-1–ACL 6-15. https://doi.org/10.1029/2001JD001236.

Hagan, M. E., and Forbes, J. M. (2003). Migrating and nonmigrating semidiurnal tides in the upper atmosphere excited by tropospheric latent heat release. J. Geophys. Res., 108, A2, 1062, doi:10.1029/2002JA009466.

He, M., Chau, J. L., Stober, G., Li, G., Ning, B., & Hoffmann, P. (2018). Relations between semidiurnal tidal variants through diagnosing the zonal wavenumber using a phase differencing technique based on two ground-based detectors. Journal of Geophysical Research: Atmospheres, 123, 4015–4026. https://doi.org/10.1002/2018JD028400.

He, M., & Chau, J. L. (2019). Mesospheric semidiurnal tides and near-12 h waves through jointly analyzing observations of five specular meteor radars from three longitudinal sectors at boreal midlatitudes. Atmospheric Chemistry and Physics, 19(9), 5993–6006. https://doi.org/10.5194/acp-19-5993-2019.

Hindley N P, Mitchell N J, Cobbett N, et al. (2022). Radar observations of winds, waves and tides in the mesosphere and lower thermosphere over South Georgia island (54 °S, 36 °W) and comparison with WACCM simulations. Atmospheric Chemistry and Physics, 22 (14): 9435–9459.

Hocking, W. K., Fuller, B., & Vandepeer, B. (2001). Real-time determination of meteor-related parameters utilizing modem digital technology. Journal of Atmospheric and Solar-Terrestrial Physics, 63(2–3), 155–169. https://doi.org/10.1016/s1364-6826(00)00138-3.

Holdsworth, D. A., I. M. Reid, and M. A. Cervera (2004), Buckland Park all-sky interferometric meteor radar, Radio Sci., 39, RS5009, doi:10.1029/2003RS003014.

Huang, F. T., H. G. Mayr, C. A. Reber, T. Killeen, J. Russell, M. Mlynczak, W. Skinner, and J. Mengel (2006), Diurnal variations of temperature and winds inferred from

https://doi.org/10.5194/egusphere-2026-1883
Preprint. Discussion started: 10 April 2026

TIMED and UARS measurements, J. Geophys. Res., 111, A10S04, doi:10.1029/2005JA011426.

Isoda, F., Tsuda, T., Nakamura, T., Vincent, R. A., Reid, I. M., Achmad, E., Sadewo, A., and Nuryanto, A. (2004). Intraseasonal oscillations of the zonal wind near the mesopause observed with medium-frequency and meteor radars in the tropics, J. Geophys. Res., 109, D21108, https://doi.org/10.1029/2003JD003378.

Jacobi, Ch., Portnyagin, Yu., Solovjova, T., et al., 1999. Climatology of the semidiurnal tide at 52 ℵN–56 ℵN from ground-based radar wind measurements 1985–1995. J Atmos Solar-Terr Phys., 61, 975–991.

Lieberman, R. S., D. A. Ortland, and E. S. Yarosh, Climatology and interannual variability of diurnal water vapor heating, J. Geophys. Res., 108(D3), 4123, doi:10.1029/2002JD002308, 2003.

Lieberman, R. S., D. M. Riggin, D. A. Ortland, S. W. Nesbitt, and R. A. Vincent (2007), Variability of mesospheric diurnal tides and tropospheric diurnal heating during 1997–1998, J. Geophys. Res., 112, D20110, doi:10.1029/2007JD008578.

Li, T., She, C. Y., Liu, H., Yue, J., Nakamura, T., and Krueger, D. A. (2009). Observation of local tidal variability and instability, along with dissipation of diurnal tidal harmonics in the mesopause region over Fort Collins, Colorado (41◦ N, 105◦ W), J. Geophys. Res.-Atmos., 114, D06106, https://doi.org/10.1029/2008jd011089.

Liu, G., Janches, D., Lieberman, R. S., Moffat-Griffin, T., Fritts, D. C., & Mitchell, N. J. (2020). Coordinated observations of 8-and 6-hr tides in the mesosphere and lower thermosphere by three meteor radars near 60 ℵS latitude. Geophysical Research Letters, 47, e2019GL086629. https://doi.org/10.1029/2019GL086629.

Liu, H. L. and Hagan, M. E. (1998). Local heating/cooling of the mesosphere due to gravity wave and tidal coupling, Geophys. Res. Lett., 25, 2941–2944, https://doi.org/10.1029/98GL02153.

Liu, H., Tsutsumi, M., & Liu, H. (2019). Vertical structure of terdiurnal tides in the Antarctic MLT region: 15-year observation over Syowa (69◦S, 39◦E). Geophysical Research Letters, 46. https://doi.org/10.1029/2019GL082155

Liu, M., Xu, J., Liu, H., and Liu, X. (2016). Possible modulation of migrating diurnal tide by latitudinal gradient of zonal wind observed by SABER/TIMED. Sci. China Earth Sci. 59, 408–417 https://doi.org/10.1007/s11430-015-5185-4.

Llamedo, P., Salvador, J., de la Torre,A., Quiroga, J., Alexander, P., Hierro,R., et al. (2019). 11 years of Rayleigh lidar observations of gravity wave activity above the southern tip of South America. Journal of Geophysical Research: Atmospheres, 124, 451–467.https://doi.org/10.1029/2018JD028673.

Kishore Kumar, G., Singer, W., Oberheide, J., Grieger, N., Batista, P.P., Riggin, D.M., Schmidt, H., Clemesha, B.R. (2014). Diurnal tides at low latitudes: radar, satellite, and model results. J. Atmos. Sol. Terr. Phys. 118, 96–105. http://dx.doi.org/10.1016/j.jastp.2013.07.005.

Kubota, M., A. Kano, H. Muramatsu, and H. Tomita, 2003: Intercomparison of Various Surface Latent Heat Flux Fields. J. Climate, 16, 670–678, https://doi.org/10.1175/1520-0442(2003)016<0670:IOVSLH>2.0.CO;2.

https://doi.org/10.5194/egusphere-2026-1883
Preprint. Discussion started: 10 April 2026

Manson, A. H., Meek, C.E., Hagan, M., et al. (1999). Seasonal variations of the semi-diurnal tides in the MLT: multi-year MF radar observations from 2 to 70 ℃N, and the GSWM tidal model. J Atmos Sol-Terr Phys., 61, 809–828.

Manson, A. H., C. M., M. Hagan, J. Koshyk, S. Franke, D. Fritts, C. Hall, W. Hocking, K. Igarashi, J. MacDougall, D. Riggin, and R. Vincent (2002). "Seasonal variations of the semi-diurnal and diurnal tides in the MLT: multi-year MF radar observations from 2-70 ℃N, modelled tides (GSWM, CMAM)." Ann. Geophys. 20: 661-677.

Manson, A. H., C. Meek, M. Hagan, X. Zhang, and Y. Luo (2004), Global distributions of diurnal and semidiurnal tides: Observations from HRDIUARS of the MLT region and comparison with GSWM-02 (migrating, nonmigrating components), Ann. Geophys., 22(5), 1529– 1548.

Manson, A. H., Meek, C. E., Chshyolkova, T., et al., (2009). Arctic tidal characteristics at Eureka (80 ℃N, 86 ℃W) and Svalbard (78 °N, 16 °E) for 2006/07: seasonal and longitudinal variations, migrating and non-migrating tides. Ann. Geophys., 27, 1153–1173, doi:10.5194/angeo-27-1153-2009.

McLandress, C., 2002a: The Seasonal Variation of the Propagating Diurnal Tide in the Mesosphere and Lower Thermosphere. Part I: The Role of Gravity Waves and Planetary Waves. J. Atmos. Sci., 59, 893–906, https://doi.org/10.1175/1520-0469(2002)059<0893:TSVOTP>2.0.CO;2.

McLandress, C., 2002b: The Seasonal Variation of the Propagating Diurnal Tide in the Mesosphere and Lower Thermosphere. Part II: The Role of Tidal Heating and Zonal Mean Winds. J. Atmos. Sci., 59, 907 - 922, https://doi.org/10.1175/15200469(2002)059<0907:TSVOTP>2.0.CO;2

Mitchell,N. J., Pancheva, D., Middleton, H., Hagan, M. (2002). Mean winds and tides in the Arctic mesosphere/lower thermosphere region and comparison with the GSWM. J Geophys Res., 106(A1), doi:10.1029/2001JA900127.

Mitchell, N. (2019). University of bath: Ascension Island Skiymet Meteor radar data (2005-2012) [dataset]. Centre for Environmental Data Analysis. https://catalogue.ceda.ac.uk/uuid/0d05cf74e17f49c2b7c5cd02faa59291.

Mitchell, N. (2021). University of bath: King Edward point Skiymet Meteor radar data (2016-2020) [dataset]. https://doi.org/10.5285/061fc7fd1ca940e7ad685daf146db08f.

Mukhtarov, P., Pancheva, D., and Andonov, B. (2009). Global structure and seasonal and interannual variability of the migrating diurnal tide seen in the SABER/TIMED temperatures between 20 and 120 km. J. Geophys. Res., 114(A2), A02309. https://doi.org/10.1029/2008JA013759

Murphy, D. J. (2003). Observations of a nonmigrating component of the semidiurnal tide over Antarctica. Journal of Geophysical Research, 108(D8), 4241. https://doi.org/10.1029/2002JD003077

Murphy, D. J., Forbes, J. M., Walterscheid, R. L., Hagan, M. E., Avery, S. K., Aso, T., et al. (2006). A climatology of tides in the Antarctic mesosphere and lower thermosphere. Journal of Geophysical Research, 111, D23104. https://doi.org/10.1029/2005JD006803

https://doi.org/10.5194/egusphere-2026-1883
Preprint. Discussion started: 10 April 2026

Oberheide, J., Wu, Q., Killeen, T. L., Hagan, M. E., & Roble, R. G. (2006). Diurnal nonmigrating tides from TIMED Doppler interferometer wind data: Monthly climatologies and seasonal variations. Journal of Geophysical Research, 111, A10S03. https://doi.org/10.1029/2005JA011491

Pancheva, D., Mukhtarov, P., Andonov, B., (2009). Global structure, seasonal and interannual variability of the migrating semidiurnal tide seen in the SABER/TIMED temperatures (2002– 2007). Ann Geophys., 27, 687–703.

Pancheva, D., P. Mukhtarov, and B. Andonov (2010), Climatology of the eastward propagating tides seen in the SABER/TIMED temperatures (2002–2007), Adv. Space Res., 46, 257–274, doi:10.1016/j.asr.2010.03.026

Pancheva, D., P. Mukhtarov, and A. K. Smith (2014), Nonmigrating tidal variability in the SABER/TIMED mesospheric ozone, Geophys. Res. Lett., 41, 4059–4067, doi:10.1002/2014GL059844.

Pancheva, D., Mukhtarov, P., Hall, C., Meek, C., Tsutsumi, M., Pedatella, N., Nozawa, S., Manson, A. (2020). Climatology of the main (24-h and 12-h) tides observed by meteor radars at Svalbard and Troms ø: Comparison with the models CMAM-DAS and WACCM-X, Journal of Atmospheric and Solar-Terrestrial Physics, doi: https://doi.org/10.1016/j.jastp.2020.105339.

Ramesh, K., Mitchell, N. J., Hindley, N. P., & Moffat-Griffin, T. (2024). Long-term variability and tendencies in mesosphere and lower thermosphere winds from meteor radar observations over Esrange (67.9 °N, 21.1 °E). Journal of Geophysical Research: Atmospheres, 129, e2023JD040404. https://doi.org/10.1029/2023JD040404.

Randall, C. E., et al. (2017), New AIM/CIPS global observations of gravity waves near 50–55 km, Geophys. Res. Lett., 44,7044–7052, doi:10.1002/2017GL073943.

Reid, I. M., McIntosh, D. L., Murphy, D. J., & Vincent, R. A. (2018). Mesospheric radar wind comparisons at high and middle southern latitudes. Earth, Planets and Space, 70(1), 84. doi:10.1186/s40623-018-0861-1.

Rienecker, M. M., Suarez, M. J., Todling, R., Bacmeister, J., Takacs, L., Liu, H., Gelaro, R. (2008). The GEOS-5 data assimilation system-documentation of versions 5.0.1, 5.1.0, and 5.2.0 (Vol. 27; Tech. Rep.). Technical Report Series on Global Modeling and Data Assimilation NASA/TM-2008-104606.

Riggin, D.M., Fritts, D.C., Jarvis, M.J., Jones, G., 1999. Spatial structure of the 12-hour wave in the Antarctic as observed by radar. Earth, Planets Space, 51, 621–628.

Sheng Z., He Y., Wang S., et al. (2025). Dynamics, chemistry, and modeling studies in the aviation and aerospace transition zone. The Innovation 6:101012.

Smith, A., 2012. Global dynamics of the MLT. Surv Geophys., 33, 1177–1230, doi: 10.1007/s10712- 012-9196-9.

Stober G, Kuchar A, Pokhotelov D, et al. (2021a). Interhemispheric differences of mesosphere–lower thermosphere winds and tides investigated from three whole-atmosphere models and meteor radar observations. Atmospheric Chemistry and Physics, 21 (18): 13855–13902.

https://doi.org/10.5194/egusphere-2026-1883
Preprint. Discussion started: 10 April 2026

Stober G, Janches D, Matthias V, et al. (2021b). Seasonal evolution of winds, atmospheric tides, and Reynolds stress components in the Southern Hemisphere mesosphere–lower thermosphere in 2019. Annales Geophysicae, 39 (1): 1–29.

Wang, J., Yi, W., Wu, J., Chen, T., Xue, X., Zeng, J., et al. (2022). Coordinated observations of migrating tides by multiple meteor radars in the equatorial mesosphere and lower thermosphere. Journal of Geophysical Research: Space Physics, 127, e2022JA030678. https://doi.org/10.1029/2022JA030678.

Wu, Q., D. A. Ortland, T. L. Killeen, R. G. Roble, M. E. Hagan, H.-L. Liu, S. C. Solomon, J. Xu, W. R. Skinner, and R. J. Niciejewski (2008a), Global distribution and interannual variations of mesospheric and lower thermospheric neutral wind diurnal tide: 1. Migrating tide, J. Geophys. Res., 113, A05308, doi:10.1029/2007JA012542.

Wu, Q., D. A. Ortland, T. L. Killeen, R. G. Roble, M. E. Hagan, H.-L. Liu, S. C. Solomon, J. Xu, W. R. Skinner, and R. J. Niciejewski (2008b), Global distribution and interannual variations of mesospheric and lower thermospheric neutral wind diurnal tide: 2. Nonmigrating tide, J. Geophys. Res., 113, A05309, doi:10.1029/2007JA012543.

Vincent, R. A., Kovalam, S., Fritts, D. C., and Isler, J. R. (1998). Long-term MF radar observations of solar tides in the low-latitude mesosphere: Interannual variability and comparisons with the GSWM. J. Geophys. Res., 103(D8), 8667–8683. https://doi.org/10.1029/98JD00482.

Xu, J., Smith, A. K., Liu, H.-L., Yuan, W., Wu, Q., Jiang, G., et al. (2009). Seasonal and quasi-biennial variations in the migrating diurnal tide observed by Thermosphere, Ionosphere, Mesosphere, Energetics and Dynamics (TIMED). Journal of Geophysical Research, 114, D13107. https://doi.org/10.1029/2008JD011298.

Yi, W., Xue, X. H., Chen, J. S., Chen, T. D., and Li, N. (2019). Quasi-90-day oscillation observed in the MLT region at low latitudes from the Kunming meteor radar and SABER. Earth Planet. Phys., 3(2), 1–11. http://doi.org/10.26464/epp2019013.

Yi W, Xue X H, Zeng J, et al. Observation of MLT region winds and tides by the USTC Mengcheng meteor radar. JUSTC, 2023, 53(5): 0501. DOI: 10.52396/JUSTC-2022-0158

Yi, Wen (2025). Monthly mean amplitudes and phases of composite zonal and meridional diurnal, semidiurnal and terdiurnal tidal components. figshare. Dataset. https://doi.org/10.6084/m9.figshare.29648918.v1

Zeng J, Yi W, Xue X, et al. (2022). Comparison between the mesospheric winds observed by two collocated meteor radars at low latitudes. Remote Sensing, 14 (10): 2354.

Zhang, R., X. Wang, and C. Wang, 2018: On the Simulations of Global Oceanic Latent Heat Flux in the CMIP5 Multimodel Ensemble. J. Climate, 31, 7111–7128, https://doi.org/10.1175/JCLI-D-17-0713.1.

Zhang, X., J. M. Forbes, and M. E. Hagan (2010), Longitudinal variation of tides in the MLT region: 2. Relative effects of solar radiative and latent heating, J. Geophys. Res., 115, A06317, doi:10.1029/2009JA014898.

https://doi.org/10.5194/egusphere-2026-1883
Preprint. Discussion started: 10 April 2026

751 Zhou, B. Z., Xue, X. H., Yi, W., Ye, H. L., Zeng, J., Chen, J. S., et al. (2022). A
752 comparison of MLT wind between meteor radar chain data and SD-WACCM
753 results. Earth and Planetary Physics, 6(5), 451–464.
754 https://doi.org/10.26464/epp2022040.